

# On Sea-Level Change in Coastal Areas

V. Courtillot<sup>1</sup>, J-L. Le Mouél<sup>1</sup>, and F. Lopes<sup>1</sup>

Université Paris Cité, Institut de Physique du globe de Paris, CNRS UMR 7154, F-75005 Paris, France

## ABSTRACT

Variations in sea-level, based on tide gauge data (**GSLTG**) and on combining tide gauges and satellite data (**GSLI**) are subjected to singular spectrum analysis (**SSA**), to determine their trends and periodic or quasi-periodic components. **GLSTG** increases by 90 mm from 1860 to 2020, a contribution of 0.56 mm/yr to the mean rise rate. Annual to multi-decadal periods of  $\sim 90/80, 60, 30, 20, 10/11,$  and  $4/5$  years are found in both **GSLTG** and **GSLI**. These periods are commensurable periods of the Jovian planets, combinations of the periods of Neptune (165 yr), Uranus (84 yr), Saturn (29 yr) and Jupiter (12 yr). These same periods are encountered in sea-level changes, motion of the rotation pole **RP** and evolution of global pressure **GP**, suggesting physical links. The first SSA components comprise most of the signal variance: 95% for **GSLTG**, 89% for **GSLI**, 98% for **GP**, 75% for **RP**. Laplace derived the Liouville-Euler equations that govern the rotation and translation of the rotation axis of any celestial body. He emphasized that one must consider the orbital kinetic moments of all planets in addition to gravitational attractions and concluded that the Earth's rotation axis should undergo motions that carry the combinations of periods of the Sun, Moon and planets. Almost all the periods found in the **SSA** components of sea-level (**GSLI** and **GSLTG**), global pressure (**GP**) and polar motion (**RP**), of their modulations and their derivatives can be associated with the Jovian planets. It would be of interest to search for data series with longer time spans, that could allow one to test whether the trends themselves could be segments of components with still longer periodicities (*e.g.* 175 yr Jose cycle).

**Key words.** Sea Level, Tide Gauges, Global Sea Pressure, Mean Pole Path

## 1. Introduction

A global rise in sea-level has become a topic of major concern for both inhabitants of coastal areas and regions of very low altitude and a huge amount of studies have been devoted to the description and understanding of evolutions in global sea-level. The problem is sometimes confusing because the definition of sea-level rise (and drop) is not always clear and unique and the observations on which it is based have been obtained with very different methods (tide gauges, GPS measurements, satellite observations). Referring to works by [Farrell and Clark \(1916\)](#), [Wu and Peltier \(1983\)](#), [Mitrovica and Milne \(2003\)](#), [Spada and Stocchi \(2006\)](#), [Spada and Stocchi \(2007\)](#), [Spada et al. \(2012\)](#), we define absolute sea-level **SL**(P,t) as the difference between (1) the distance from the center of mass of Earth to the sea surface, at time t and location P, and (2) the distance from the center of mass of Earth to the sea bottom (solid Earth), that is the water depth, at the same time t and location P:

$$\mathbf{SL}(P,t) = R_{ss}(P,t) - R_{se}(P,t) \quad (1)$$

The evolution of sea level between time t and a reference time  $t_r$  is simply:

$$\begin{aligned} \mathbf{SLE}(P,t) &= \mathbf{SL}(P,t) - \mathbf{SL}(P,t_r) \\ &= [R_{ss}(P,t) - R_{se}(P,t)] - [R_{ss}(P,t_r) - R_{se}(P,t_r)] \end{aligned} \quad (2)$$

which can be rearranged as:

$$\mathbf{SLE}(P,t) = [R_{ss}(P,t) - R_{ss}(P,t_r)] - [R_{se}(P,t) - R_{se}(P,t_r)] \quad (3)$$

In that form, changes in sea level are the difference between changes in altitude of the sea surface (*i.e.* the geoid), which are measured by tide gauges in coastal areas and changes in the altitude of the solid Earth that can be measured at GPS stations (*e.g.* [Blewitt et al. \(2016\)](#); [Hammond et al. \(2021\)](#)). The geoid term  $[R_{ss}(P,t) - R_{ss}(P,t_r)]$  is modeled as:  $\frac{G}{\gamma}(P,t) + c(t)$ , where G is the full gravitational potential, G gravity at the Earth surface and c(t) stands for changes in masses at the surface, including ice melting ([Lambeck 2005](#)).

Despite the actual complexity of consequences of the (apparently simple) law of attraction of masses, [Laplace \(1799\)](#) was able to build a full theory of celestial mechanics. He wrote a whole volume (the book IV of his Treatise) on the oscillations of the sea and of the atmosphere. Laplace showed that in order for sea-level to be in equilibrium, the sum of forces had to be zero, resulting eventually in the famous Liouville-Euler system of partial differential equations. Tides were understood to be second-order oscillations, whose phases and amplitudes could be computed. The mathematical stage was set for the study of changes in sea-level.

The early 1930s saw a period of active interest in the determination of sea level and its changes, and the physical causes of these changes. [Nomitsu and Okamoto \(1927\)](#)

attributed **SL** variations in the Sea of Japan to variations in density and atmospheric pressure. [Marmor \(1927\)](#) noted an annual oscillation at the tide gauges of Seattle and San Francisco that he also linked to meteorological phenomena. After a decade of additional observations, [Jacobs \(1939\)](#) and [LaFond \(1939\)](#) concluded that there was indeed a general rise in sea-level. Several explanations were considered: insolation from the Sun, meteorological tides, water density, changes in geography and geology of ocean basins. None was found completely satisfactory. [McEwen \(1937\)](#) envisioned a complex mechanism, with evaporation in the summer and precipitation in winter affecting global sea-level. Further study showed that these annual variations were in fact in phase in all observation stations, and the idea had to be dropped. Only the pressure patterns, hence the winds remained as a potential cause of periodic **SL** variations.

By the end of the 1970s and early 1980s, the principal cause of sea-level rise came to be attributed to a major phase of warming having resulted in melting of the northern hemisphere ice caps. [Peltier and Andrews \(1976\)](#) and [Nakiboglu and Lambeck \(1980\)](#) elaborated on the theory of post-glacial isostatic rebound. The global warming of the atmosphere that took place over the past 150 years or so was attributed to anthropic release of greenhouse gases, contributing to the melting of glaciers and a rise in **SL** ([Etkins and Epstein 1982](#); [Gornitz et al. 1982](#); [Lambeck and Nakiboglu 1984](#); [Meier 1984](#); [Peltier and Tushingham 1989](#); [Douglas 1991, 1992, 1997](#)).

Our knowledge of sea-level and its variations in the 19th century and up to the present is primarily based on observations made by tide gauges. They provide the first half of equation (3), that is  $[R_{ss}(P,t) - R_{ss}(P,t_r)]$ . One of the longest series comes from the Brest (France) tide gauge, established in 1807 and still in function. [Le Mouél et al. \(2021\)](#) have recently analyzed the Brest data and in parallel Earth's pole positions (from the IERS, 1845-2019), submitting both of them to singular spectral analysis (**SSA**). The first **SSA** components of both series, *i.e.* the trends, are very similar, with a major acceleration event near 1900 and sea-level lagging pole motion by 5-10 years. **SSA** components with periods 1 yr, ~11 yr and 5.4 yr are common to the two series. An important feature is a 0.5 yr component that is present in sea-level but absent from pole motion. The remarkable similarity of the two trends and their phase lag suggests a causal relationship opposite to what is generally accepted.

The primary aim of the present paper is to apply the same analysis to the global data base of tide gauges. The tide gauge data are maintained by the Permanent Service of Mean Sea Level<sup>1</sup> (**PSMSL**). Measurements of coastal sea level are available at 1548 sites ; the raw data at all sites are shown in Figure 1.

The second half of equation 3, that is vertical land motion  $VLM = [R_{se}(P,t) - R_{se}(P,t_r)]$ , can be accessed through GPS measurements. These allow far better coverage of Earth surface but cover a much shorter span of time, in general at most 30 yr. For that reason, only “recent” trends covering that period can be accessed. A very thorough analysis of these data has recently been published by [Hammond et al. \(2021\)](#). The data base is maintained by the Nevada Geodetic Laboratory, with 19286 sites scattered throughout the globe, and is called Median Interannual Difference Adjusted for Skewness (**MIDAS**)<sup>2</sup>.

Since the beginning of the 1990s sea-level has also been monitored by series of altimetric satellites that have allowed much denser global coverage but (as is the case for GPS measurements) over a short time range of 30 years. A number of recent papers have attempted to combine these very different data sets, resulting in various global sea-level (**GSL**) curves (*e.g.* [Church and White \(2011\)](#); [Hammond et al. \(2021\)](#)). Interest in these **GSL** curves has focused on their trends, acceleration, annual and inter-annual variations, and on the mechanisms responsible for these variations.

We have recently successfully applied the method of singular spectral analysis (**SSA**; see [Golyandina and Zhigljavsky \(2013\)](#); [Lemmerling and Van Huffel \(2001\)](#); [Golub and Reinsch \(1971\)](#)) to a number of geophysical and heliophysical time series. **SSA** decomposes any time series into a sum of components, a trend (that may or may not be present) and stationary quasi-periodic components. We have explained the method in a number of papers ([Lopes et al. 2017](#); [Le Mouél et al. 2020a](#)). For instance, oscillations (pseudo-cycles) of ~160, ~90, ~60, ~22 and ~11 yr are found in series of sunspot numbers (*e.g.* [Gleissberg \(1944\)](#); [Jose \(1965\)](#); [Coles et al \(1980\)](#); [Charvatova and Strestik \(1991\)](#); [Usoskin \(2017\)](#); [Le Mouél et al. \(2020b\)](#); [Courtillot et al \(2021\)](#)) as well as in a number of terrestrial phenomena ([Wood and Lovett 1974](#); [Mörth and Schlamming 1979](#); [Schlesinger and Ramankutty 1994](#); [Lau and Weng 1995](#); [Scafetta 2010](#); [Courtillot et al 2013](#); [Scafetta 2016](#); [Lopes et al. 2017](#); [Le Mouél et al. 2019a,b, 2020a](#); [Scafetta et al. 2020](#); [Cionco et al 2021](#); [Lopes et al. 2021](#); [Scafetta 2021](#); [Lopes et al. 2022](#)), in particular sea-level ([Jevrejeva et al. 2006](#); [Chambers et al. 2012](#); [Chen et al. 2014](#); [Wahl and Chambers 2015](#); [Le Mouél et al. 2021](#)). These particular periods (or periodicities) are of special interest, as they are members of the family of commensurable periods of the Jovian planets acting on Earth and Sun ([Mörth and Schlamming 1979](#); [Scafetta et al. 2020](#); [Courtillot et al 2021](#); [Lopes et al. 2021](#); [Bank and Scafetta 2022](#)). These values are indeed close to the revolution periods of Neptune (165 yr), Uranus (84 yr), Saturn (29 yr) and Jupiter (12 yr) and several of their commensurable periods (see *f.i.* Table 1 in [Lopes et al. \(2021\)](#)).

In section 2 of this paper, we discuss the tide gauge records and perform a **SSA** of these. In section 3, we discuss and an-

<sup>1</sup> <https://www.psmsl.org/data/obtaining/complete.php>

<sup>2</sup> <http://geodesy.unr.edu/velocities/>

alyze the time series of vertical land motion (VLM) based on GPS measurements. In section 4, we submit some global sea-level (GSL) curves that include satellite observations to SSA. We compare and discuss the results of these analyses in section 5 and conclude in section 6.

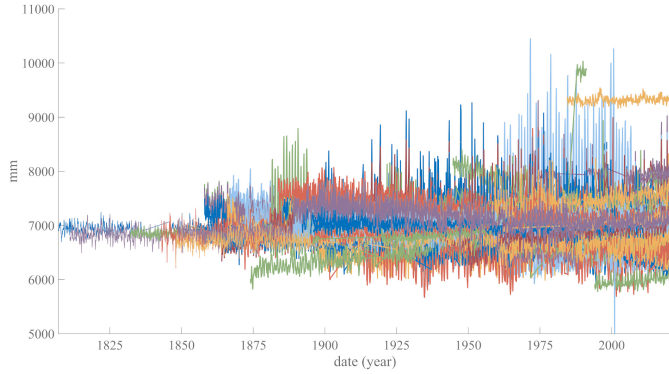


Fig. 1: The full tide gauge data base (1548 tide gauges of PSMSL series).

## 2. SSA of tide gauge records time series (ie $[R_{ss}(\mathbf{P},t) - R_{ss}(\mathbf{P},t_r)]$ )

Drawing on a recent paper by Le Mouél et al. (2021), in which we analyzed the record from the Brest tide gauge since 1807, using SSA to extract its main components, we propose to build a global sea-level curve covering the past 200 years using data from tide gauges only (GSLTG). We are aware of the uncertainties due to geography and tectonics but are interested in subjecting the original data to as little manipulation as possible.

We have selected the recordings from 31 stations (Table fig. 4), on the basis of two criteria: the longest possible span of time and the best possible, if still too restrained, spatial coverage (Figure 2).

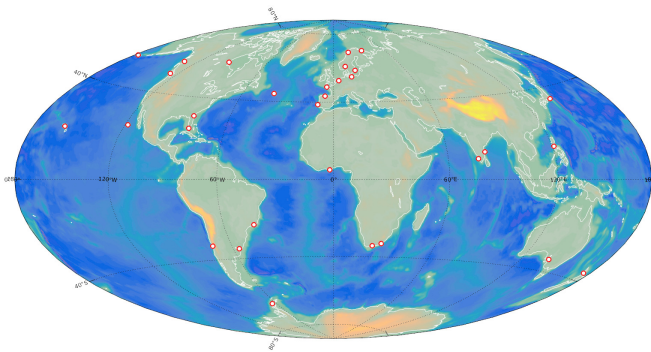


Fig. 2: Map showing the locations of tides gauges used to build the GSLTG series.

We have also performed the analyses that follow on the full database (1548 tide gauge stations): this results in increased

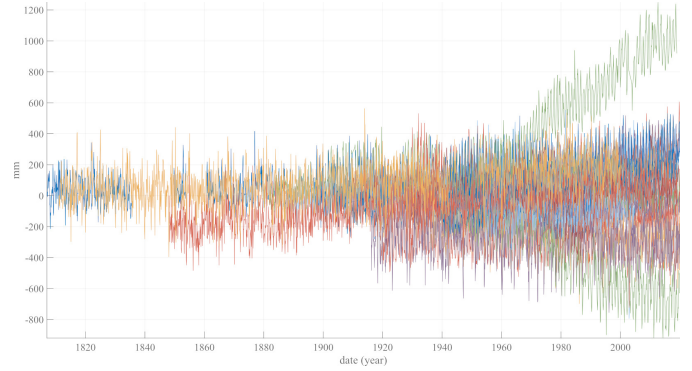


Fig. 3: Superposition of data series from the 31 tide gauges listed in Table fig. 4.

dispersion without changing what can be drawn from the selection of 31 stations. The raw data from the 31 stations are all displayed without any filtering or processing, except for the fact that the first value has been subtracted, so that all series begin with a zero and only relative vertical variations of SL are displayed (Figure 3).

The two tide gauges that have large slopes (plotted in green in Figure 3), one positive (Manila, S. Harbor, Philippines) and one negative (Churchill, Canada) (see Table fig. 4 outline a funnel shape. The funnel undergoes rapid growth after 1950, with a total amplitude of 2 m, determined by the two extrema at Manila and Churchill. The annual oscillation, first identified by Marmer (1927), has an amplitude on the order of 200 mm (peak to trough) for all tide gauges. The individual data points are shown in Figure 5a.

We next determine a smooth mathematical model of the mean sea-level variations as a function of time, in a least squares sense (e.g. Menke (1989)). For a mathematical representation of this smooth model, we can choose between polynomials, sine functions, exponentials, or splines. We select sine functions, based on our previous experience with the Brest data (Le Mouél et al. 2021) and for reasons that will appear in the discussion. We add sine components progressively, until no more significant information is brought by the new component (in the sense of the Akaike criterion, see Glattig et al. (2007) used in Courtillot et al (2013)). In the present case, this leads to a model consisting of 8 sine components. This model is shown with the data in Figure 5a and enlarged in Figure 5b.

The model of Figure 5a represents the mean variation common to all 31 tide gauges. At first glance it consists in an annual oscillation, with peak to trough amplitude around 100 mm and a rather constant overall mean value. Figure 5b shows more precisely the modulations of this amplitude. The remaining scatter of data points can be assigned to local or regional variability. We call this model GSLTG. The GSLTG curve is then analyzed using SSA. The analysis yields a sum of components with (pseudo-) periods of 1 yr, 90 yr, 60 yr, 80 yr, 0.5 yr and 20 yr (in order of decreasing amplitudes). They are shown (in order of decreasing period) in Figures 6 (see also Table fig.7). The leading annual component has an amplitude (peak to trough) of 80 mm and undergoes a (longer than centennial) modulation

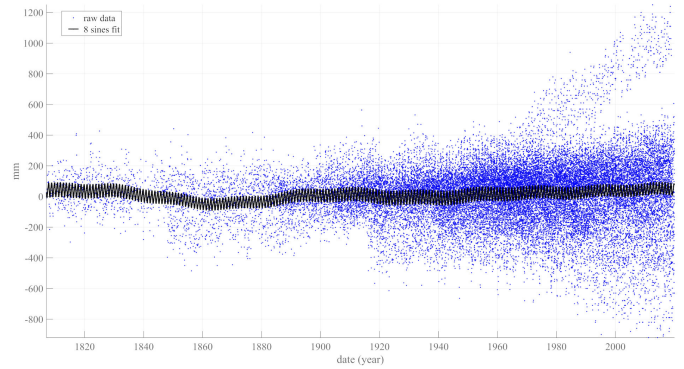
Tide Gauge Site	Lat (°)	Lon (°)
Adak Sweeper Cove	51.863	-176.632
Argentine Islands	-65.246	-64.257
Auckland	-36.843	174.769
Brest	48.382	4.494
Churchill	58.767	-94.183
Chennai	13.100	80.300
Cochin	9.967	76.267
East- London	-33.027	27.932
Fernandina Beach	30.672	-81.465
Honolulu	21.307	-157.867
Ketchikan	55.332	-131.625
Key West	24.555	-81.806
Knysna	-34.049	23.046
Lisbon	38.700	-9.133
Marseille	43.279	5.354
Maasluis	51.918	4.25
Manila, S. harbor	14.583	120.967
Mera	34.919	139.825
Montevideo	-34.900	-56.250
Narvik	68.428	17.426
Oslo	59.909	10.735
Polyarny	69.200	33.483
Port Adelaide	-34.780	138.481
Rio de Janeiro	-22.933	-43.133
Swinoujście	53.917	14.233
Takoradi	4.885	-1.745
Tofino	49.150	-125.917
Tuapse	44.100	39.067
Valparaiso	-33.027	-71.626
Visby	57.639	18.284
Xiamen	24.450	118.067

Fig. 4: List of tides gauges selected in this study to build the GSLTG series.

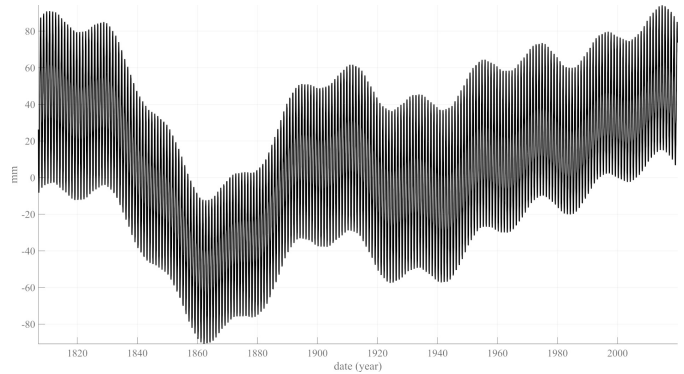
with 10 mm amplitude. The next two components (90 and 80 yr) both have an amplitude of 40 mm, and the next three about 15 mm. Taken together, they capture 95% of the total variance. The trend itself can be modeled with only 3 sine functions with periods 160, 90 and 30 yr.

### 3. Introducing the GPS vertical land motion time series (the $[R_{se}(\mathbf{P},t) - R_{se}(\mathbf{P},t_r)]$ ).

As noted above, the GPS data series of VLM are all shorter than 30 years, which makes it impossible to directly combine them with the tide gauge data that are far longer on average and allow one to explore much longer periods. For lack of being able to do better, one at least can calculate a recent (present) trend, applying a simple linear regression to the GPS data. And a simple linear regression of all the series shown in Figure 3 allows a comparison and combination of the gauge and VLM data: Figure 8 shows the respective histograms of the slopes of the 1548 gauges and of the GPS at the same (or close by)



(a) Data points from the 31 tide gauges used in building GSLTG and their sinusoidal fit, with 8 sine waves.



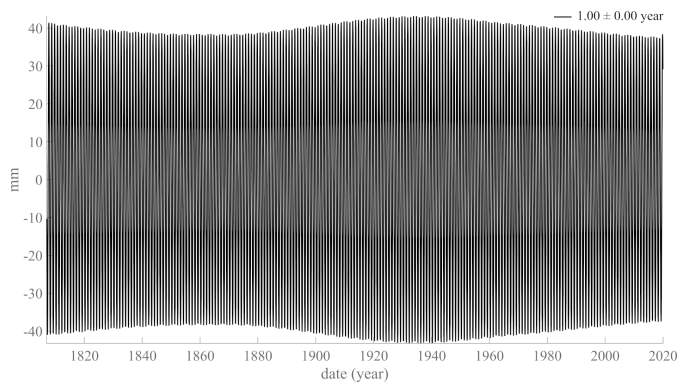
(b) The fit (black curve) of Figure 5a with an enlarged ordinate scale.

Fig. 5: Fit of the 31 tide gauges.

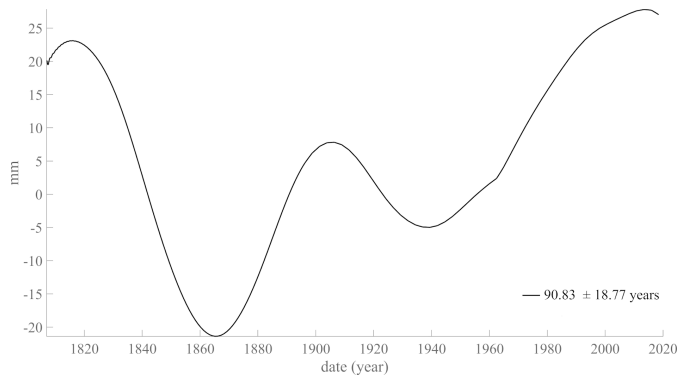
coastal locations (Figure 9). The median for tide gauges is +2.0 mm/yr and 92.7 % of gauges have slopes between -10 and +10 mm/yr; the median for VLM is -0.6 mm/yr and 96.0 % of the values are between -10 and +10 mm/yr. The locations and values of the tide gauges and the VLM are plotted respectively in Figure 9a and Figure 9b. Over a large part of the coastal areas, the tide gauge signal and the VLM appear to be opposite in sign, that is anti-symmetrical (e.g. North America, the Mediterranean region). The results of this analysis are in full agreement with the thorough study of Hammond et al. (2021); where water rises the land tends to subside and vice versa.

If we assume that the recent (30 yr) VLM at Brest remained the same from 1807 to the present, then we can evaluate the mean sea level rise with respect to the Earth's center of mass (equation 3) as 1.5 mm/yr. This rough estimate is in full agreement with a series of recent studies (e.g. Tsimplis and Baker (2000); Marcos and Tsimplis (2008); Wahl et al. (2013); White et al. (2014); Wahl and Chambers (2015); Hammond et al. (2021); Le Mouél et al. (2021)).

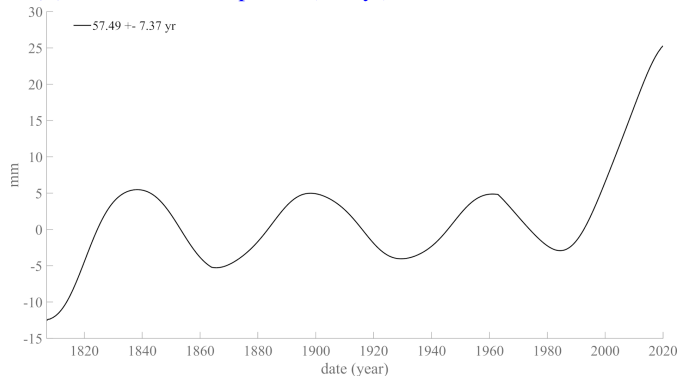
The MIDAS data base provides the slopes of the GPS data over their duration (life time), which can range from 2 to over 20 years. Hammond et al. (2021) argue that, apart from tectonic events, these give an accurate idea of VLM. For each tide gauge, we fit straight line segments to sea level data in the same



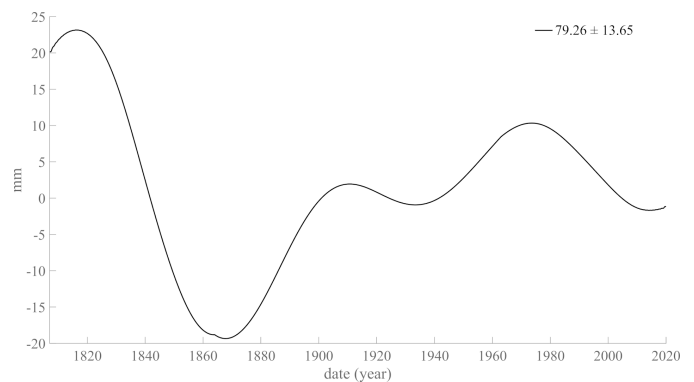
(a) First SSA component (1 yr) of the GSLTG data series of Figure 5b



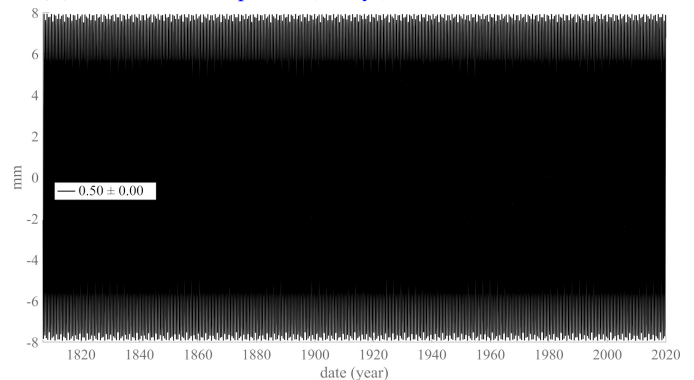
(b) Second SSA component (~90 yr) of the GSLTG data series.



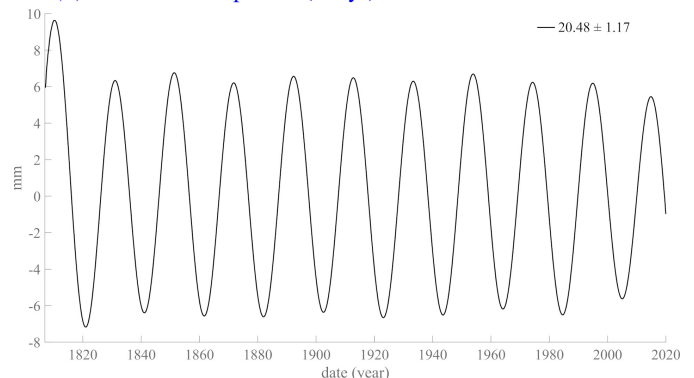
(c) Third SSA component (~60yr) of the GSLTG data series



(d) Fourth SSA component (~80 yr) of the GSLTG data series.



(e) Fifth SSA component (0.5 yr) of the GSLTG data series.



(f) Sixth SSA component (~20 yr) of the GSLTG data series.

Fig. 6: The first six most important components extracted from GSLTG

way (though over a much longer duration between 3 and 217 years).

#### 4. SSA of GSL curves obtained with inclusion of satellite data

As far as we are interested in the long term rise of sea level, and its quasi-periodic components, but do not have VLM data over this long term, we can still analyze with SSA a number of global sea-level curves available from the literature.

We select first that by Church and White (2011), Figure 10. These authors estimate the rise in global average sea level from a combination of satellite altimeter data for 1993–2009 with coastal and island sea-level (tide gauge) measurements from 1880 to 2009. Variations of GSL as a function of time are

provided by NASA<sup>3</sup>. The SSA of the resulting curve **GSLI** (1 for long) yields a trend and components at  $54.5 \pm 8.7$ ,  $19.4 \pm 1.7$ ,  $10.1 \pm 0.6$ ,  $3.9 \pm 0.1$  and  $31.0 \pm 5.5$  yr (Table fig. 7 and Figure??) in order of decreasing amplitude (or roughly, given the uncertainties, trend, 60, 20, 11, 4 and 30 yr). These components are shown in Figure 09 (in order of decreasing period); their sum amounts to 89.4% of the series total variance (Figure 10). The 3.9 yr component could correspond to the second harmonic of the Schwabe cycle (Le Mouél et al. 2020b). Note that the prominent 1 and 0.5 yr variations have been filtered out by Church and White (2011).

<sup>3</sup> [https://podaac-tools.jpl.nasa.gov/drive/files/allData/merged\\_0lt/L2/TP](https://podaac-tools.jpl.nasa.gov/drive/files/allData/merged_0lt/L2/TP)

Planet	Associated periods (yr)	SSN pseudo cycles	Church and White (GSLI)	Beckley et al (GSLs)	This study (GSLTG)
Earth	0.5 1.0			0.49 ± 0.01, 1.0 ± 0.02	0.5 ± 0.0, 1.0 ± 0.0
Jupiter	11.85 (Schwabe) 5.92	10.56, 11.3, 13.43 5.30, 5.52	10.15 ± 0.58		10.64 ± 1.17 5.36 ± 0.13
Saturn	31.44 15.72	35.56 15.31	30.96 ± 5.55		32.75 ± 9.30
Uranus	83.97 (Gleissberg)	90.03		15.36 ± 4.70	90.83 ± 18.77 79.26 ± 13.65
Neptune	164.78 (Jose) 83.39	131.02, 190.25 90.03			
Jupiter Saturn	9.79, 21.64 (Hale)	9.98, 21.42	19.41 ± 1.74		20.48 ± 1.17
Uranus Neptune	36.06, 47.91	35.56, 45.21			
Uranus Neptune	40.40, 124.37	45.21, 131.02			
3	4	57.29, 67.08	54.46 ± 8.68		57.49 ± 7.37

Fig. 7: Commensurate periods of the Jovian planets Mörth and Schlamminger (1979); Lopes et al. (2021). Periods of components extracted by SSA from sunspot series SSN, GSLI, GSlS and GSLTG are highlighted in red.

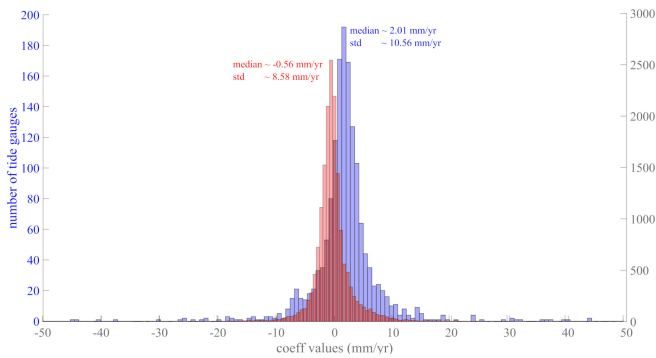
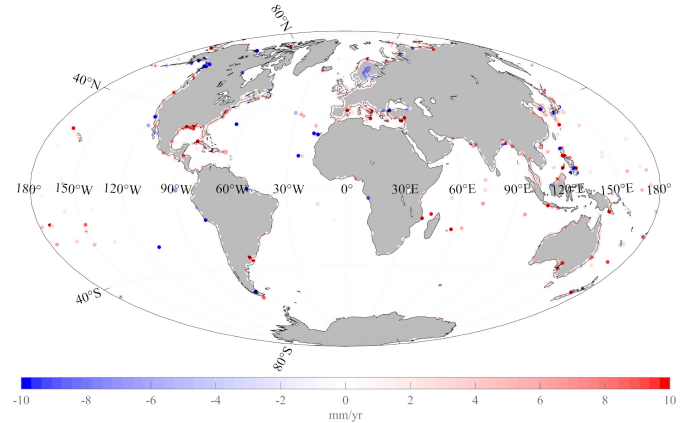


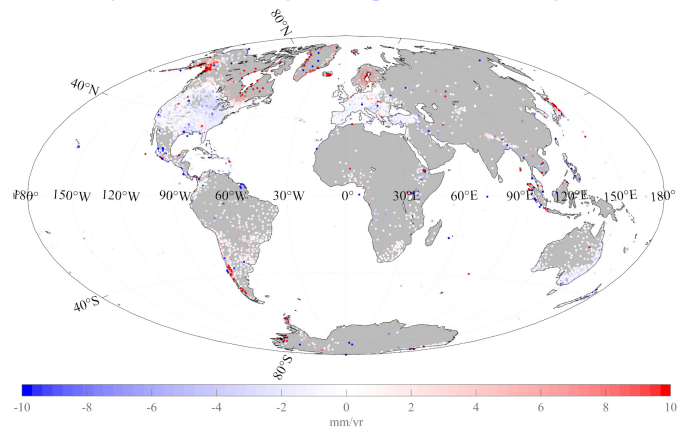
Fig. 8: Superposition of the histogram of recent slopes of 1548 tide gauges with that of the MIDAS (GPS) data (from Hammond et al. (2021)).

Since the 1880-2009 **GSLI** incorporates two very different data sets (measurements from tide gauges and satellites), we have resumed the analysis for the 1993-2009 **GSLs** (s for short) based on satellite data only. For details on the structure of the data we refer the reader to Beckley et al (2015). For explanations on how the data set has been created from 27 years of altimetric measurements by the successive satellites TOPEX/Poseidon (T/P), Jason-1, Jason-2 and Jason-3, we refer the reader to Beckley et al (2010, 2017). The global mean sea-level data consist in several sets of time series, some with “Global Isostatic Adjustment applied”, some “GIA not applied”. The latter (without GIA) is shown in Figure 12, from January 1993 to August 2020, with a sampling interval of 9.92 days.

The **SSA** of the resulting curve **GSLs** yields a trend and components at  $1.00 \pm 0.02$ ,  $0.49 \pm 0.01$ ,  $3.06 \pm 0.25$ ,  $15.4 \pm 4.7$ ,  $1.50 \pm 0.05$ ,  $6.06 \pm 0.73$  yr in order of decreasing amplitude (or roughly, given the uncertainties, trend, 15-20, 6, 3, 1.5, 1 and 0.5 yr). These components are shown in Figure 13 (in order of decreasing period); their sum amounts to 87.3% of the series total variance (Figure 12). The sum of the seven first components extracted by **SSA** is plotted as a red curve. The 6.1, 3.1 and 1.5 yr quasi periods could correspond to harmonics of the Schwabe cycle (cf. Le Mouél et al. (2020b), Table 1).



(a) The locations of tide gauges and values of the local slope of sea-level change. Color code ranges from positive (red) to negative (blue).



(b) The locations of GPS sites and the local changes (slopes) of vertical land movement (VLM) from the MIDAS data base. Color code same as in Figure 9a

Fig. 9: Comparison of GPS and tide gauges slopes.

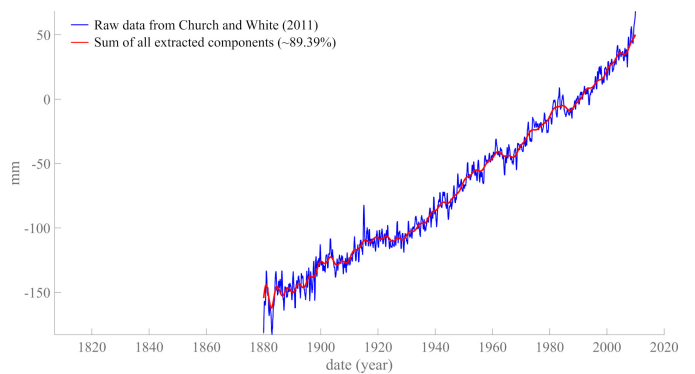
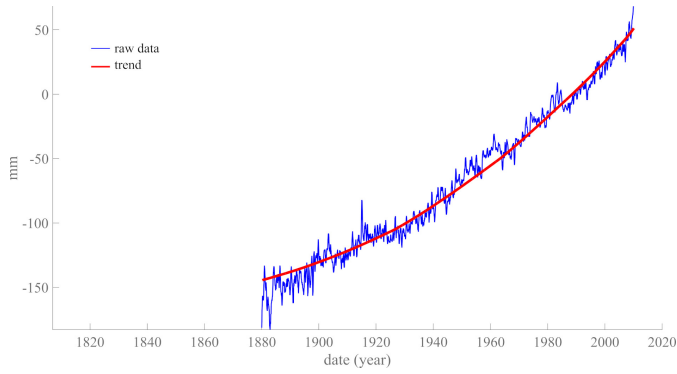


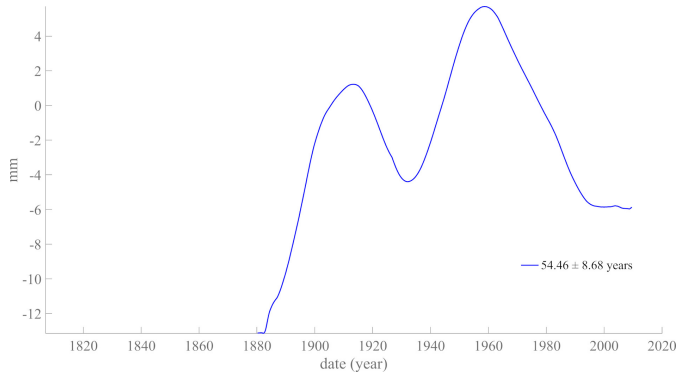
Fig. 10: Global Sea Level **GSLI** curve from Church and White (2011) in blue. Sum of first 6 components extracted by **SSA**, red curve.

## 5. Discussion

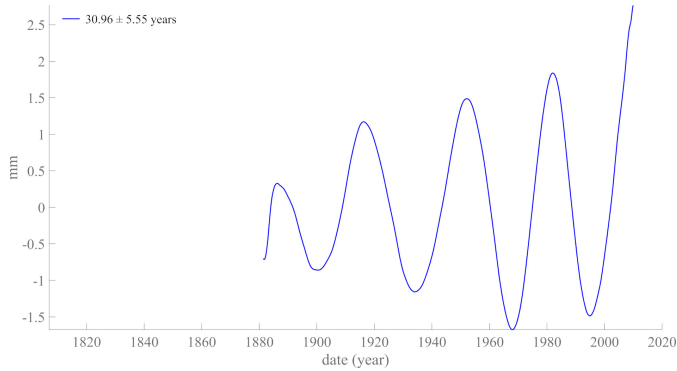
5.1 Components shared by **GSLI**, **GSLTG** and **SSN**. Despite the fact that one is included in the other, the **GSLI** and **GSLs** series do not share many characteristics (cf. Table fig. 7). Their trends are similar and they both have significant



(a) The first SSA component (trend, in red) superimposed on the GSLI data series.



(b) Second SSA component (~ 60 yr pseudo-period) of the GSLI data series.

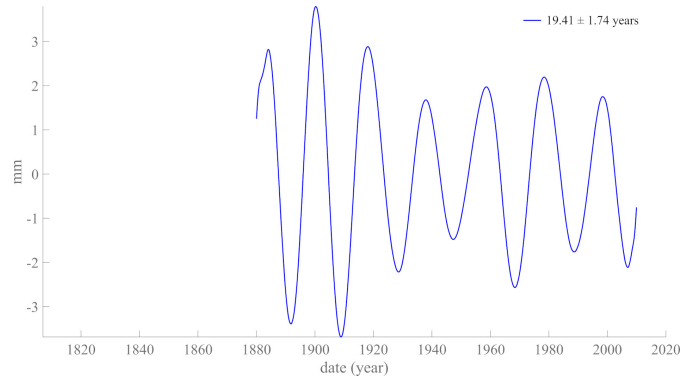


(c) Third SSA component (~ 30 yr pseudo-period) of the GSLI data series.

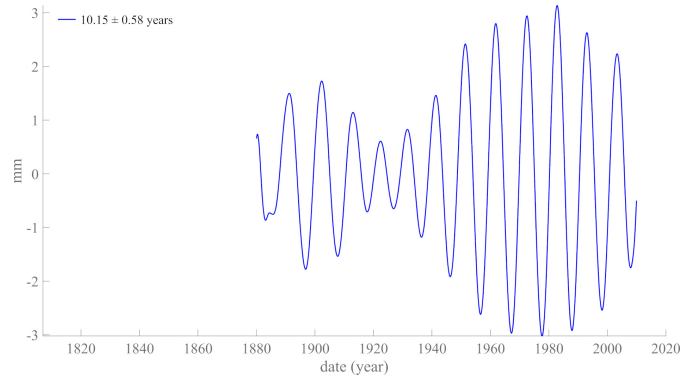
1-yr and 6-month components, but the two series do not share other quasi- periodic components (unless the 15 yr component of **GSLs** can be considered as the same as the 20 yr component of **GSLI**, given uncertainties). Actually, the span of the **GSLs** data is only 27 yr and should not be used to identify components with periods longer than, say, 27/2 or ~15 yr.

In stark contrast, **GSLI** shares seven components with **GSLTG**: a trend, 60, 30, 20, 10, 1 and 0.5 yr components (*cf.* Table fig. 7).

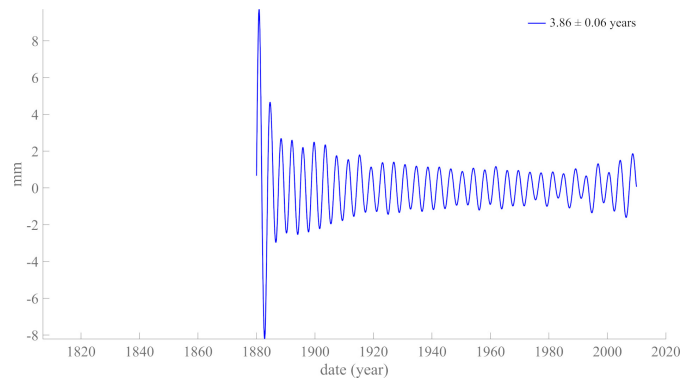
Le Mouël et al. (2019b) and Courtillot et al (2021) have calculated the SSA components of the sunspot number **SSN**, a characteristic of solar activity. Four components of **SSN** are



(d) Fourth SSA component (~ 20 yr pseudo-period) of the GSLI data series.



(e) Fifth SSA component (~ 11 yr pseudo-period) of the GSLI data series.



(f) Sixth SSA component (~ 4 yr pseudo-period) of the GSLI data series.

Fig. 11: First six components extracted by SSA from GSLI data series.

found in **GSLI** (60, 30, 20, 10 yr) and six in **GSLTG** (90, 60, 20, 30, 10, 5 yr), taking into account the uncertainties (*f.i.*  $10.15 \pm 0.58$  and  $10.64 \pm 1.17$  are both considered equivalent to the **SSN** packet at 10.6 and 11.3 yr).

A puzzling observation is that the amplitude of the annual component of **GSLs** is only 8 mm peak to trough (Figure 13b), when tide gauges record a mean amplitude an order of magnitude larger (80 mm; Figure 6a). This could be due to the fact that tide gauges are located in shallow waters where wave amplitude is amplified; in any case this is where sea-level is

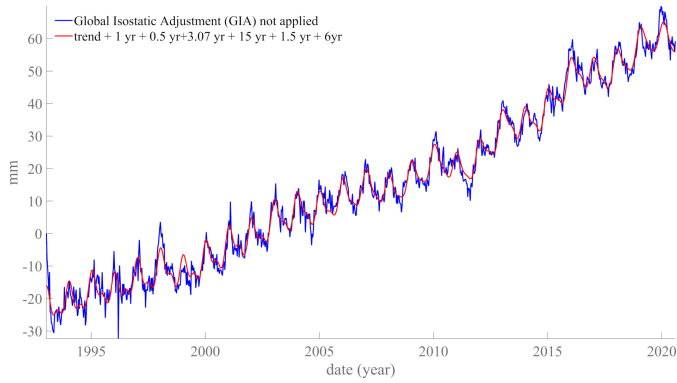
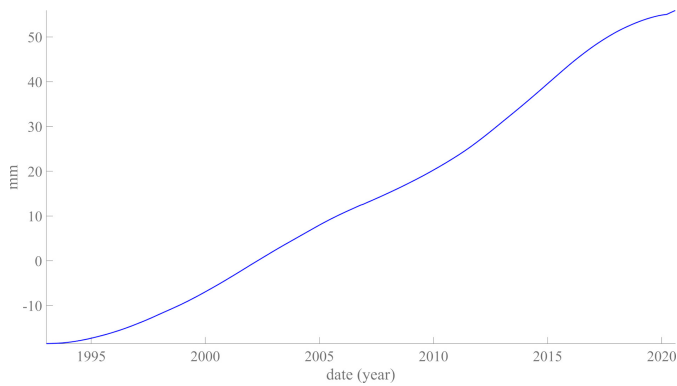
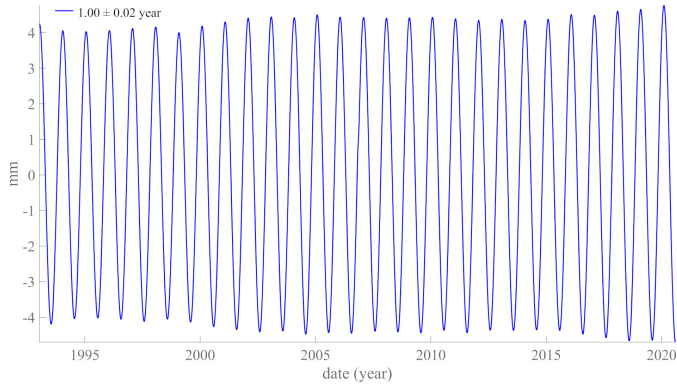


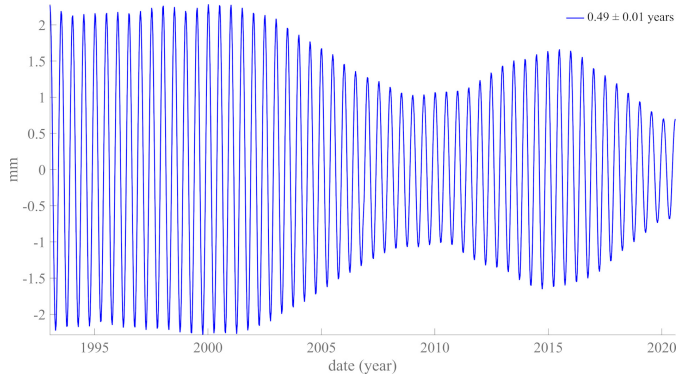
Fig. 12: Global Sea Level GSLs (blue curve). Sum of the first seven SSA components (red curve).



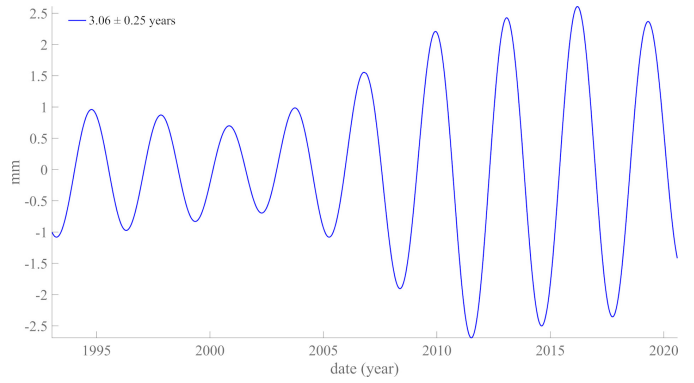
(a) First SSA component (trend) of the GSLs data series of Figure 12.



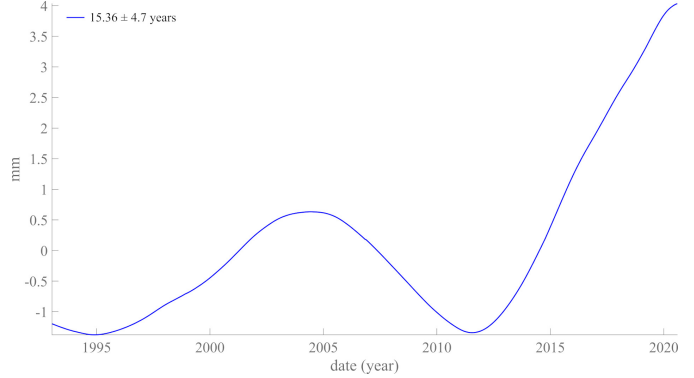
(b) Second SSA component (1 yr) of the GSLs data series.



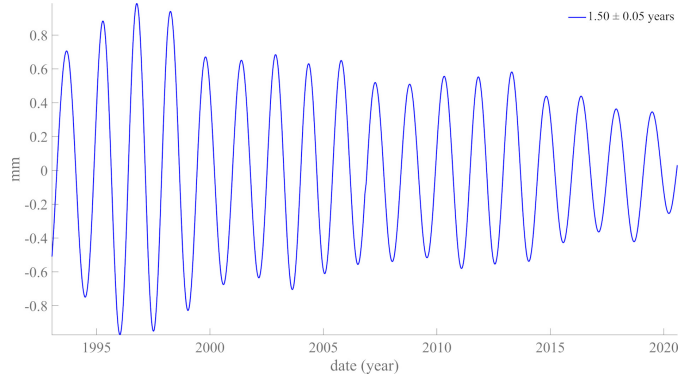
(c) Third SSA component (0.5 yr) of the GSLs data series



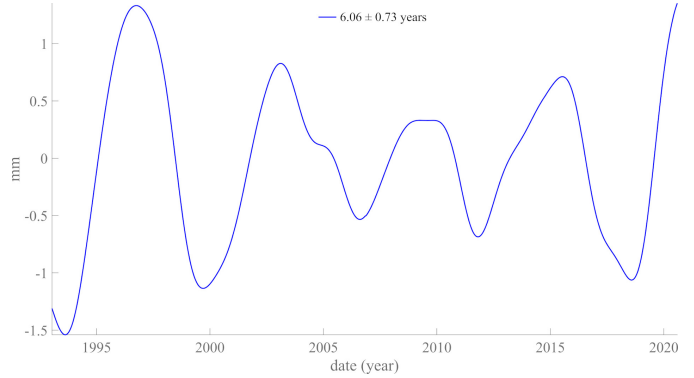
(d) Fourth SSA component (3 yr) of the GSLs data series



(e) Fifth SSA component (15 yr) of the GSLs data series.



(f) Sixth SSA component (1.5 yr) of the GSLs data series



(g) Seventh SSA component (6 yr) of the GSLs data series.

Fig. 13: First seven components extracted by SSA from GSLs data series.



relevant to human activities. The trend amplitude between 1860 and 2020 is 80 mm for **GSLTG** (Figure 5b) and more than 200 mm for **GSLI** (Figure 10). Moreover, with a **GSLTG** curve extending over two centuries, we see that the trend of the shorter series **GSLs** could actually be part of a longer cycle (on the same order as the  $\sim 90$  year Gleissberg cycle).

**5.2 Comparison with global pressure GP**. Thus, **SSA** reveals that **GSLI** and **GSLTG** share many characteristics that could constrain the mechanisms that control both series of sea-level change. In order to strengthen this hypothesis, one can try to find whether some other geophysical phenomenon would possess similar characteristic features, with the same spectral signatures. We have searched whether the Earth's global mean pressure (**GP**) meets these requirements. A series of monthly mean atmospheric pressure (everywhere in the world) is available as of 1846 (Allan andt Ansell 2006). It can be accessed through the Met Office Hadley Centre <sup>4</sup> website under the name HadSPL2. Following Laplace's work on the subject of the spatial and temporal stability of pressure (Laplace (1799), book IV, chap 4, page 294), we build a series of monthly global pressure **GP** and submit it to **SSA**: the first 4 components, *i.e.* the trend followed by periods of 1 yr, 6 months and  $\sim 25$  yr, account for 98% of the total variance. Thus, **GSLTG** and **GP** share three major components at  $\sim 20/25$  yr, 1 yr and 6 months. Comparisons between some features of **GSLTG** and **GP** are illustrated in Figure 14. The annual and semi-annual components match in phase and frequency and are slightly modulated with a time constant on the order of a century or more. Both series have  $\sim 20/25$  yr components that drift, one with respect to the other. Interestingly, the derivative of the trend of pressure **GP** matches the trend of **GSLTG**, suggesting a relation of the form **GSLTG**  $\sim$  (d/dt) **GP**. Also, the ratios of the amplitudes of the various **SSA** components of **GSLTG** and **GP** are approximately constant (Table fig. 15). Sea level and pressure respond in similar ways at all time scales.

**5.3 Comparison with the mean motion of the rotation pole (RP)**. It is generally accepted (*e.g.* Nakiboglu and Lambeck (1980)) that the mean motion of the rotation pole (**RP**) and the mean sea-level (be it **GSLTG** or **GSL**) belong to the same family, because of the reorganization of surface masses due to pole motion. Because the Liouville-Euler equations are a linear differential system of second order, one understands the resemblance between **RP** and both **GSLTG** or **GSL**, at least at the longer periods. Can analysis of the **RP** series bring additional light on the question of the forcing of sea-level (we refer the reader to earlier work on polar motion by Lopes et al. (2017); Le Mouél et al. (2020a); Lopes et al. (2021))?

The series of data describing the rotation pole coordinates (**RP**) is maintained by the International Earth Rotation and

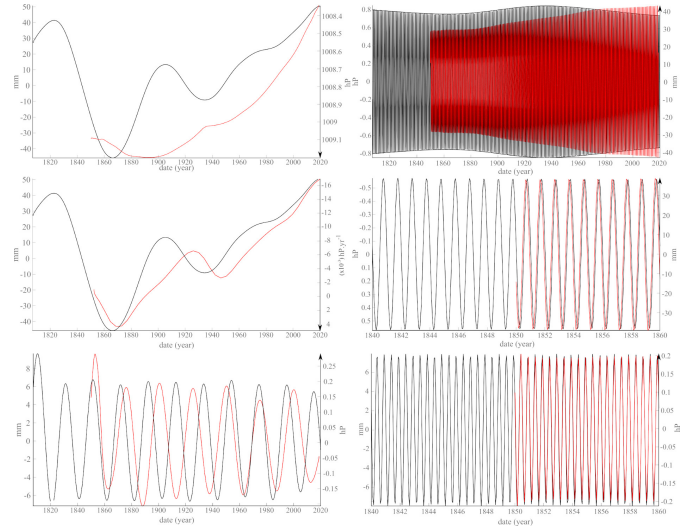


Fig. 14: Top left, the superposition of the trends of **GSLTG** (in black) and **GP** (in red). Middle left, the superposition of the trend of **GSLTG** (in black) and the first derivative of the trend of **GP** (in red). Bottom left, the  $\sim 20$  yr components of **GP** (red) and **GSLTG** (black). Top right and middle right (a zoom), the annual oscillations of **GSLTG** (black) and **GP** (red). Bottom right, the semi-annual cycles of **GP** (red) and **GSLTG** (black).

Cycles (yr)	GSLTG		
	Sea Level (mm)	Pressure (hPa)	ratio (hPa/mm)
Trend	45	0.8	0.019
20-30	18	0.45	0.025
1	80	1.6	0.020
0.5	16	0.3	0.019

Fig. 15: Ratios of **SSA** components of **GP** to **GSLTG** with the same periods (see text).

Reference Systems Service (**IERS**)<sup>5</sup>. Two series of measurements of pole coordinates  $m_1$  and  $m_2$  are provided by **IERS** under the codes EOP-C01-IAU1980 and EOP-14-C04. The first one runs from 1846 to July 1st 2020 with a sampling rate of 18.26 days, and the second runs from 1962 to July 1st 2020 with daily sampling. Figure 16 displays the trends (top) and derivatives (bottom) of the rotation pole (**RP**) coordinates  $m_1$  and  $m_2$  together with those of **GSLTG** (1807-2020). There is a suggestive anti-correlation between the trend of **GSLTG** and the derivative of the trend of  $m_2$  (**GSLTG**  $\sim$  (d/dt) **RP**), with the former leading the latter by several decades (Figure 16, lower left). This behavior was noted for the Brest tide gauge by Le Mouél et al. (2020a). This is yet another line of observational evidence that the sea-level curve based on tide

<sup>4</sup> <http://www.metoffice.gov.uk/hadobs/hadspl2/data/download.html>

<sup>5</sup> <https://www.iers.org/IERS/EN/DataProducts/EarthOrientationData/eop.html>

gauges has an underlying physical mechanism.

The three main components of pole motion **RP**, *i.e.* the Markovitch drift, the Chandler free oscillation (that has never yet been detected in sea level) and the annual forced oscillation, carry more than 75% of the signal's total energy (variance) (Lopes et al. 2017, 2021, 2022). Lopes et al. (2017) also showed the presence of other components at 22 yr (Hale), 11 yr (Schwabe) and a 5.5 yr harmonic. The order of magnitude of these solar components is  $10^{-12}$  to  $10^{-14}$  rad.sec<sup>-1</sup>, that is 1 to 4 orders of magnitude smaller than the main components ( $10^{-11}$  to  $10^{-10}$  rad.sec<sup>-1</sup>). In Courtillot et al (2021), Le Mouël et al. (2021), Lopes et al. (2021), it has been shown that the derivative of the Markovitch component includes the 90 yr (Gleissberg) cycle as its trend. Lopes et al. (2021) have identified some other components that also appear in the SSN sunspot series (Courtillot et al 2021). We limit ourselves to the shared (quasi-) periods of 90, 22, 11, 5.5, 1.4 (Chandler) and 1 year.

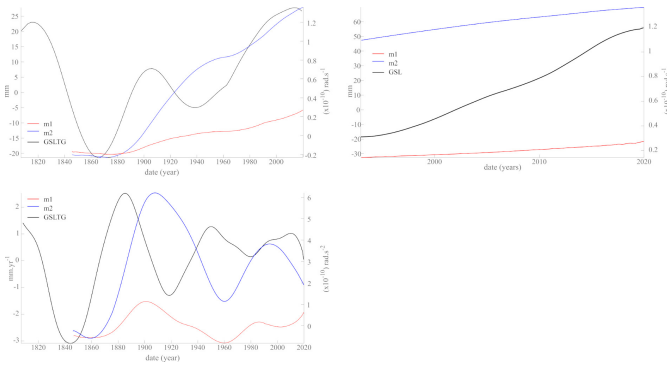


**Fig. 16:** Trends (top) and their derivatives (bottom) of the rotation pole (**RP**) coordinates  $m_1$  (red) and  $m_2$  (blue) compared with those for **GSLTG** (left; 1807-2020).

**5.4 The Liouville-Euler system and solar components in sea-level.** The Liouville-Euler system of equations can be written (*cf.* Lambeck (2005); chapters 3 and 4):

$$\begin{aligned} (1/\sigma_r) \frac{d\mathbf{m}}{dt} + \mathbf{m} &= \mathbf{f} \\ \frac{dm_3}{dt} &= f_3 \end{aligned} \quad (4)$$

$\frac{d\mathbf{m}}{dt} = m_1 + i * m_2$ , where  $(m_1, m_2)$  are the coordinates of motion of the Earth's rotation pole (**RP**) and  $\mathbf{f} = f_1 + i * f_2$  and  $f_3$  are the excitation functions. These are explicitly written in Lambeck (2005), chapter 4, system 4.1.1, page 47. These functions belong to three distinct families: masses, motions (of masses), and imposed forces (torques). Parameters  $(m_1, m_2, m_3)$  provide a global scalar for pole motion, and the excitation functions are also global. Because coupled system (4) is linear, any periodic component found in  $(m_1, m_2, m_3)$  data/observations must also be present in  $(f_1, f_2, f_3)$ .

If system (4) does apply, since variations in sea-level are the motion part of the excitation functions, and since the Gleissberg cycle (90 yr) and annual components have been found, one should also find the Chandler (1.4 yr) component. In the same way, Moreira et al. (2021) identify an 11 yr oscillation, Jevrejeva et al. (2006) a 22 yr oscillation and Chambers et al. (2012) another one at 60 yr (solar, *cf.* Courtillot et al (2021)) with weak amplitude in polar motion (*cf.* Lopes et al. (2021, 2022)). Thus, cycles that are commonly associated to the Sun are also detected in sea level, though they are a very weak component of polar motion.

**5.5 Planetary forcings.** Laplace predicted that all terrestrial masses should be under the influence of other celestial bodies, at much longer periods (though he did not have the data to demonstrate it experimentally). For these longer durations, planets were the potential culprits. If one studies durations that are short compared to a decade, the 11 yr component will be included in the trend. In the same way, if one looks at the variations shorter than 5 days, the 28 day lunar cycle will be included in the trend. This is particularly true for the fluid envelopes. In Courtillot et al (2021), we showed that sunspots, that move on the external fluid envelope of the Sun, include components with periods that can be linked to planetary ephemerids (commensurable periods of the Jovian planets, as proposed by Mörth and Schlamming (1979), namely ~ 165 yr (José cycle, associated with Neptune), ~90 yr (Gleissberg cycle, associated with Uranus), ~30 yr (Saturn), ~ 22 yr (Hale cycle, a Jupiter/Saturn commensurability), ~ 11 yr (Schwabe cycle, associated with Jupiter), *etc.*

The solid Earth acts as an integrator (*e.g.* Lambeck (2005), Chapter 3) at the longer periods (*e.g.* Lopes et al. (2021)), but reacts almost instantaneously to the shorter periods (*e.g.* Le Mouël et al. (2019c)). The effects are large in the former case, less so in the latter. As pointed out by Laplace (1799), Book IV, Chapters 4 and 5, because the atmosphere and oceans are fluids with low viscosity, they actually behave as solid envelopes at the longer periods. This is for instance the reason why the annual oscillations observed on tide gauges (Figures 13) have similar amplitudes. To this response is added the response described by the Liouville-Euler equations. It is used for instance by Nakiboglu and Lambeck (1980), who consider that there is a reorganization of surface masses when the inclination of the Earth's rotation axis evolves in space. External forces influence polar motion and this should also be seen in sea-level and pressure. We do find signatures of these influences in the trends (directly or through their derivatives), the most energetic components. The apparent rise of sea-level is similar to the pattern of polar motion: this is why, like others, we find this funnel pattern of tide gauges. The mass of the system is constant; this agrees with the fact that the pressure variation remains constant and linked with sea-level. Under the hypothesis of common external forcing (common to the solid Earth and its fluid envelopes) this would explain why the derivative of the trend of

**GP** (with sign reversed) and the trend of **GSLTG** match quite well (Figure 14, middle left).

## 6. Summary and Concluding Remarks

In the present paper, we have first analyzed variations in the geoid, using tide gauge data for the time span 1807-2020 (**GSLTG**) and variations of global sea level combining tide gauges and satellite data (**GSLI**; Church and White (2011)), then, with much better spatial coverage but a much more restricted time span (1993-2020), satellite-only data (**GSLs**, Beckley et al (2015)). Our main goal has been to determine the trends and successive periodic or quasi-periodic components of these time series, using the powerful method of singular spectrum analysis (**SSA**) that we have used, with interesting results, in a series of previous papers (Lopes et al. 2017, 2021; Le Mouél et al. 2019a,b, 2021; Courtillot et al 2021).

Since satellite data are first corrected using tide gauges, we have analyzed the tide gauge data at 71 gauge stations separately (series **GSLTG**). We see all kinds of behavior, with increasing, stable or decreasing mean values (trend), giving the complete data set a funnel shape. The resulting **GLSTG** mean oscillates about an almost constant value. From 1860 to 2020, the trend increases by 90 mm, or a contribution to the mean rise rate of 0.56 mm/yr.

Our observations are compatible with previous results also based on tide gauge data but using different methods: Gornitz et al. (1982) Figure 02, Warrick and Oerlemans (1990) Figures 9.1 and 9.2 and Douglas (1992) Figure 03 show the funnel shaped distribution of the data with values in agreement with **GSLTG**.

**SSA** analysis of the **GSLTG** series identifies components with celestial periods already found when analyzing the Brest tide gauge data (Le Mouél et al. 2021). We have shown (Table fig. 15) that the ratios of amplitudes of **SSA** components (trend, 20-30 yr, 1 yr, 0.5 yr) of **GSLTG** vs global pressure **GP** are almost constant (at 0.02 hPa/mm). This observation supports the idea that tide gauge data contain significant information on the physical links between mean pressure and (geoid) sea-level.

The longer (annual to multi-decadal) periods we have encountered in the **GSLTG** and **GSLI** sea-level curves in the present study have already been encountered in a number of geophysical and heliophysical time series. These periods (or quasi-periods) are ~90/80, 60, 30, 20, 10/11, and 4/5 years. They can be compared to the commensurable periods of the Jovian planets acting on Earth and Sun as proposed by Mörth and Schlamming (1979). The combination of the revolution periods of Neptune (165 yr), Uranus (84 yr), Saturn (29 yr) and Jupiter (12 yr) and several commensurable periods makes additional pseudo-cycles of 60 and 20 yr appear in sunspots (Le Mouél et al. 2020a; Courtillot et al 2021) as well as in a number of terrestrial phenomena (Mörth and Schlamming 1979; Courtillot et al 2013; Scafetta 2016; ?; Lopes et al. 2017; Le Mouél et al. 2020a; Lopes et al. 2021; Scafetta

et al. 2020; Bank and Scafetta 2022), in particular sea-level (Chambers et al. 2012; ?; Parker 2013; Parker and Ollier 2016). It is therefore not a surprise to find Jovian periods in **GSLTG**. Even trends could be part of commensurate cycles longer than the time span over which the data are available.

The (often joint) periods encountered in the sea-level changes, motion of the rotation pole **RP** and evolution of global pressure **GP** and the relations between some of their trends (as determined using **SSA**) suggest that there may be physical links and causal relationships between these geophysical phenomena and the time series of observations available. The ubiquitous presence of many common components in the variations of many natural phenomena (that a priori might seem largely unrelated) has led us to return to the general forcing envisioned by Laplace (1799) and to the full theory he developed. In his 1799 Treatise of Celestial Mechanics, Laplace derived the Liouville-Euler partial differential equations that describe the rotation and translation of the rotation axis of any celestial body, and showed that the only thing that influences the rotation of celestial bodies is the action of other celestial bodies. Laplace emphasized that one must consider the orbital kinetic moments of all planets in addition to gravitational attractions and concluded that the Earth's rotation axis should undergo motions with components that carry the periods or combinations of periods of the Sun, Moon and planets (particularly Jovian planets).

In Lopes et al. (2021, 2022), we tested Laplace's theoretical results using observations that have accumulated since his time. In Courtillot et al (2021), we gave evidence of the driving influence of the planets (mainly the Jovian planets) on the Earth's rotation axis (Lopes et al. 2021), and on solar activity, through exchanges of angular momentum. In the present paper, we have extended the analysis to changes in global sea-level, as measured by tide gauges (**GSLTG**), and we have in addition shown that there were several shared periodic components with global pressure **GP** and Earth's rotation axis **RP**.

Laplace's treatment shows that the kinetic moments of planets act both directly on Earth and on the Sun's fluid external layers, and perturb its rotation, hence its revolution and eventually the Earth's axis of rotation **RP**. The **SSA** analysis of the envelopes of the derivatives of the three first polar motion components yields a number of additional periods that belong to the series of commensurable periods, among which 70 yr, 60 yr (Saturn; also found in global temperatures and oceanic oscillations), 40 yr (a commensurable revolution period of the four Jovian planets), 30 yr (Saturn), 22 yr (Jupiter and Solar). The same is true for the first three **SSA** components of sunspot series **SSN** (trend or Jose 175 year cycle, linked to Neptune; 11 yr Schwabe cycle, linked to Jupiter; and 90 yr Gleissberg cycle, linked to Uranus). Almost all the (quasi-) periods found in the **SSA** components of sea-level (**GSLI** and **GSLTG**), global pressure (**GP**) and polar motion (**RP**), of their modulations, and of their derivatives can be associated with the Jovian planets (Table fig. 15). They complement the list of **SSA** quasi-periodic

and periodic components that are found in **GSLI**, **GSLTG**, **GP**, **RP** and **SSN** (90, 60, 30, 20, 10, 5, 1 and 0.5 years) and can all be associated with planetary forcings, as envisioned by Laplace. In particular planetary forcing factors are likely causally responsible for many of the components of sea-level variations as measured by tide gauges. It is of particular interest to search for high-quality data series on longer time intervals, that can allow one to test whether the trends themselves could be segments of components of even longer periodicities (e.g. 175 yr Jose cycle). In any case the first **SSA** components of the series analyzed in this paper comprise a large fraction of the signal variance: 95% for the first 6 components of **GSLTG**, 89% for the first six components of **GSLI**, 87% for the first six components of **GSLs**, 98% for the first four components of **GP**, 75% for the first three components of **RP**. It is clear that one should attempt to physically model these series with this set of periods (**SSA** components) before trying to invoke alternate sources (forcing functions).

## References

- Allan, R. & Ansell, T., “A new globally complete monthly historical gridded mean sea level pressure dataset (HadSLP2): 1850–2004”, *Journal of Climate*, 19(22), 5816–5842, 2006
- Bank, M. J. & Scafetta, N., “Scaling, mirror symmetries and musical consonances among the distances of the planets of the solar system”, *arXiv preprint arXiv:2202.03939*, 2022
- Beckley, B.D., N. P. Zelensky, S. A. Holmes, F. G. Lemoine, R. D. Ray, G. T. Mitchum, S. D. Desai & S. T. Brown, “Assessment of the Jason-2 Extension to the TOPEX/Poseidon, Jason-1 Sea-Surface Height Time Series for Global Mean Sea Level Monitoring”, *Marine Geodesy*, Vol 33, 2010.
- Beckley, B., Zelensky, N.P., Holmes, S.A., Lemoine, F.G., Ray, R.D., Mitchum, G.T., Desai, S. & Brown, S.T., “Global Mean Sea Level Trend from Integrated Multi-Mission Ocean Altimeters TOPEX/Poseidon Jason-1 and OSTM/Jason-2 Version 3”, *Ver. 3. PO.DAAC, CA, USA*, Dataset accessed, 2015
- Beckley, B. D., Callahan, P. S., Hancock III, D. W., Mitchum, G. T., & Ray, R. D., “On the “Cal Mode” Correction to TOPEX Satellite Altimetry and Its Effect on the Global Mean Sea Level Time Series.”, *Journal of Geophysical Research: Oceans*, 122(11), 8371–8384, 2017.
- Blewitt, G., Kreemer, C., Hammond, W. C., & Gazeaux, J., “MIDAS robust trend estimator for accurate GPS station velocities without step detection”, *Journal of Geophysical Research: Solid Earth*, 121(3), doi.org/10.1002/2015JB012552, 2054–2068, 2016
- Chambers, D. P., Merrifield, M. A. & Nerem, R. S., “Is there a 60-year oscillation in global mean sea level?”, *Geophysical Research Letters*, 39(18), 2012
- Charvatova, I. & Strestik, J., “Long-term variations in duration of solar cycles”, *Bulletin of the Astronomical Institutes of Czechoslovakia*, 42, 90–97, 1991
- Chen, Xianyao, Ying Feng, & Norden E. Huang. ”Global sea level trend during 1993 - 2012.”, *Global and Planetary Change*,112: 26–32, 2014
- Church, J. A. & White, N. J., “Sea-level rise from the late 19th to the early 21st century”, *Surveys in geophysics*, 32(4), 585–602, doi.org/10.1007/s10712-011-9119-1, 2011
- Cionco, R.G., Kudryavtsev, S.M. & Soon, W.H., ”Possible Origin of Some Periodicities Detected in Solar Terrestrial Studies: Earth’s Orbital Movements.”, *Earth and Space Science*, 8.8: e2021EA001805, doi.org/10.1029/2021EA001805, 2021
- Coles, W. A., Rickett, B. J., Rumsey, V. H., Kaufman, J. J., Turley, D. G., Ananthakrishnan, S. A. J. W., ... & Sime, D. G., “Solar cycle changes in the polar solar wind”, *Nature*, 286(5770), 239–241, 1980
- Courtillot, V., Le Mouél, J-L, Kossobokov, V, Gibert, G. and Lopes, F., “Multi-Decadal Trends of Global Surface Temperature: A Broken Line with Alternating 30 yr Linear Segments?”, *Atmospheric and Climate Sciences*, Vol.3, No.3, Article ID:34080, 2013
- Courtillot, V., Lopes, F. & Le Mouél, J-L., “On the prediction of solar cycles”, *Solar Physics*, 296.1, 1–23, 2021.
- Douglas, B. C., “Global sea level rise”, *Journal of Geophysical Research: Oceans*, 96.C4: 6981– 6992, 1991
- Douglas, B. C., “Global sea level acceleration”, *Journal of Geophysical Research: Oceans*, 97(C8), 12699–12706, 1992
- Douglas, B. C., “Global sea rise: a redetermination”, *Surveys in Geophysics*, 18(2), 279–292, 1997
- Etkins, R., & Epstein, E. S., “The rise of global mean sea level as an indication of climate change”, *Science*, 215(4530), 287–289, 1982
- Farrell, W. E. & Clark, J. A., “On post glacial sea level”, *Geophysical Journal International*, 46(3), doi.org/10.1111/j.1365-246X.1976.tb01252.x, 647–667, 1976
- Glattig, G., Kletting, P., Reske, S. N., Hohl, K., & Ring, C. “Choosing the optimal fit function: Comparison of the Akaike information criterion and the F test”, *Medical physics*, 34(11), 4285–4292, 2007.
- Gleissberg, W., “A table of secular variations of the solar cycle”, *Terrestrial Magnetism and Atmospheric Electricity*, 49(4), 243–244, 1944
- Golub, G. H., & Reinsch, C., ”Singular value decomposition and least squares solutions”, *In Linear algebra* (pp. 134–151), Springer, Berlin, Heidelberg, 1971
- Golyandina, N. and Zhigljavsky, A., “Singular Spectrum Analysis for time series”, (Vol. 120). Berlin: Springer, 2013
- Gornitz, V., Lebedeff, S., & Hansen, J., “Global sea level trend in the past century”, *Science*, 215(4540), 1611–1614, 1982
- Hammond, W. C., Blewitt, G., Kreemer, C., & Nerem, R. S., GPS Imaging of Global Vertical Land Motion for Studies of Sea Level Rise, *Journal of Geophysical Research: Solid Earth*, 126(7), e2021JB022355, doi.org/10.1029/2021JB022355, 2021
- Jacobs, W. C., “Sea level departures on the California coast as related to the dynamics of the atmosphere over the North Pacific Ocean”, *J. mar. Res.*, 2(3), 181–194, 1939
- Jevrejeva, S., Moore, J. C., Grinsted, A. & Woodworth, P. L., ”Recent global sea level acceleration started over 200 years ago?”, *Geophysical Research Letters*, 35(8), 2006

- Jose, P. D., "Sun's motion and sunspots", *The Astronomical Journal*, 70(3), 193-200, 1965
- LaFond, E. C., "Variations of sea level on the Pacific coast of the United States", *J. Mar.Res.*, 2(1), 17-29, 1939.
- Lambeck, K. & Nakiboglu, S. M., "Recent global changes in sealevel", *Geophysical Research Letters*, 11(10), 959-961, doi.org/10.1029/GL011i010p00959, 1984
- Lambeck, K., "The Earth's variable rotation: geophysical causes and consequences", *Cambridge University Press*, 2005
- Laplace, P. S., "Traité de mécanique céleste", *de l'Imprimerie de Crapelet*, 1799
- Lau, KM. & Hengyi Weng. "Climate signal detection using wavelet transform: How to maketime series sing", *Bulletin of the American meteorological society*, 76.12: 2391-2402, 1995
- Le Mouél, J. L., Lopes, F. & Courtillot, V., "A solar signature in many climate indices", *Journal of Geophysical Research: Atmospheres*, 124(5), 2600-2619, 2019a
- Le Mouél, J. L., Lopes, F. & Courtillot, V., "Singular spectral analysis of the aa and Dst geomagnetic indices", *Journal of Geophysical Research: Space Physics*, 124(8), 6403-6417, 2019b
- Le Mouél, J. L., Lopes, F., Courtillot, V. & Gibert, D., "On forcings of length of day changes: From 9-day to 18.6-year oscillations", *Physics of the Earth and Planetary Interiors*, 292, 1-11, 2019c
- Le Mouél, J. L., Lopes, F. & Courtillot, V., "Characteristic time scales of decadal to centennial changes in global surface temperatures over the past 150 years", *Earth and Space Science*, 7(4), doi.org/10.1029/2019EA000671, 2020a
- Le Mouél, J. L., Lopes, F. & Courtillot, V., "Solar turbulence from sunspot records", *Monthly Notices of the Royal Astronomical Society*, 492(1), 1416-1420, doi.org/10.1093/mnras/stz3503, 2020b
- Le Mouél, J. L., Lopes, F. & Courtillot, V., "Sea-Level Change at the Brest (France) Tide Gauge and the Markowitz Component of Earth's Rotation", *Journal of Coastal Research*, doi.org/10.2112/JCOASTRES-D-20-00110.1, 2021
- Lemmerling, P. & S. Van Huffel, "Analysis of the structured total least squares problem for hankel/toeplitz matrices", *Numerical Algorithms* 27 (1), 89–114. 16, 2001.
- Lopes, F., Le Mouél, J. L. & Gibert, D., "The mantle rotation pole position. A solar component", *Comptes Rendus Geoscience*, 349(4), 159-164, doi.org/10.1016/j.crte.2017.06.001, 2017
- Lopes, F., Le Mouél, J. L., Courtillot, V. & Gibert, D., "On the shoulders of Laplace", *Physics of the Earth and Planetary Interiors*, 316, 106693, 2021
- Lopes, F., Courtillot, V., Mouél, J. L. & Gibert, D., "On two formulations of polar motion and identification of its sources", arXiv preprint [arXiv:2204.11611](https://arxiv.org/abs/2204.11611), 2022
- McEwen, G. F., "Some energy relations between the sea surface and the atmosphere". *Yale Univ*, 1937
- Marcos, M., & Tsimplis, M. N., Coastal sea level trends in Southern Europe, *Geophysical Journal International*, 175(1), 70-82, doi.org/10.1111/j.1365-246X.2008.03892.x, 2008
- Marmer, H. A., "Tidal datum planes (No. 135)", *US Government Printing Office*, 1927.
- Meier, M. F., "Contribution of small glaciers to global sea level", *Science*, 226(4681), 1418-1421, 1984.
- Menke, W., "Geophysical data analysis: Discrete inverse theory", *volume 45 of International geophysics series*, 1989
- Mitrovica, J. X. & Milne, G. A., "On post-glacial sea level: I. General theory", *Geophysical Journal International*, 154(2), 253-267, doi.org/10.1046/j.1365-246X.2003.01942.x, 2003
- Moreira, L., Cazenave, A., and Palanisamy, H. "Influence of interannual variability in estimating the rate and acceleration of present-day global mean sea level." *Global and Planetary Change*, 199, 103450, 2021
- Mörth, H. T., & Schlamminger, L., "Planetary motion, sunspots and climate", *Solar-terrestrial influences on weather and climate* (pp. 193-207), *Springer*, Dordrecht, 1979
- Nakiboglu, S. M., & Lambeck, K., "Deglaciation effects on the rotation of the Earth", *Geophysical Journal Inter.*, 62(1), 49-58, doi.org/10.1111/j.1365-246X.1980.tb04843.x, 1980
- Nomitsu, T., & Okamoto, M., "The causes of the annual variation of the mean sea level along the Japanese coast", *Memoirs of the College of Science, Kyoto Imperial University. Series A*, 10(3), 125-161, 1927
- Parker, A., "Sea level trends at locations of the United States with more than 100 years of recording", *Natural Hazards*, 65(1), 1011-1021, 2013
- Parker, A., & Ollier, C. D., "Coastal planning should be based on proven sea level data", *Ocean & Coastal Management*, 124, 1-9, 2016
- Peltier, W.R. & Andrews, J.T, "Glacial-isostatic adjustment – I", *The forward problem*, *Geophysical Journal Inter.*, 46(3), 605-646, 1976
- Peltier, W. R. & Tushingham, A. M., "Global sea level rise and the greenhouse effect: might they be connected?", *Science*, 244(4906), 806-810, 1989
- Scafetta, N., "Empirical evidence for a celestial origin of the climate oscillations and its implications", *Journal of Atmospheric and Solar-Terrestrial Physics*, 72(13), 951-970, 2010
- Scafetta, N., "High resolution coherence analysis between planetary and climate oscillations", *Advances in Space Research*, 57.10 (2016): 2121-2135, 2016
- Scafetta, N., Milani, F. & Bianchini, A., "A 60-year cycle in the Meteorite fall frequency suggests a possible interplanetary dust forcing of the Earth's climate driven by planetary oscillations", *Geophysical Research Letters*, 47(18), e2020GL089954, 2020
- Scafetta, N., "Reconstruction of the Interannual to Millennial Scale Patterns of the Global Surface Temperature", *Atmosphere*, 12(2), 147, 2021
- Schlesinger, M. E. & Ramankutty, N., "An oscillation in the global climate system of period 65–70 years", *Nature*, 367(6465), 723-726, 1994
- Spada, G. & Stocchi, P., The sea level equation, theory and numerical examples, (pp. 1-96). *Aracne Editrice*, 2006
- Spada, G. & Stocchi, P., SELEN: A Fortran 90 program for solving the sea-level equation, *Computers & Geosciences*,

- 33(4), 538-562, doi.org/10.1016/j.cageo.2006.08.006, 2007
- Spada, G., Melini, D., Galassi, G., & Colleoni, F., Modeling sea level changes and geodetic variations by glacial isostasy: the improved SELEN code, *arXiv preprint*, [arXiv:1212.5061](https://arxiv.org/abs/1212.5061), 2012.
- Tsimplis, M. N. & Baker, T. F., "Sea level drop in the Mediterranean Sea: an indicator of deep water salinity and temperature changes?", *Geophysical Research Letters*, 27(12), 1731-1734, 943 doi.org/10.1029/1999GL007004, 2000
- Usoskin, I. G., "A history of solar activity over millennia", *Living Reviews in Solar Physics*, 14(1), 3, 2017
- Wahl, T., Haigh, I. D., Woodworth, P. L., Albrecht, F., Dillingh, D., Jensen, J., ... & Wöppelmann, G., Observed mean sea level changes around the North Sea coastline from 1800 to present, *Earth-Science Reviews*, 124, 51-67, doi.org/10.1016/j.earscirev.2013.05.003, 2013
- Wahl, T., & Chambers, D. P., Evidence for multidecadal variability in US extreme sea level records, *Journal of Geophysical Research: Oceans*, 120(3), 1527-1544, 954 doi.org/10.1002/2014JC010443, 2015.
- Warrick, R. A., and J. Oerlemans, "Sea level rise ", 257-281, 1990
- White, N. J., Haigh, I. D., Church, J. A., Koen, T., Watson, C. S., Pritchard, T. R., ... & Tregoning, P., "Australian sea levels-Trends, regional variability and influencing factors", *Earth-Science Reviews*, doi.org/10.1016/j.earscirev.2014.05.011, 136, 155-174, 2014
- Wood, C. A., & Lovett, R. R., Rainfall, drought and the solar cycle. *Nature*, 251(5476), 594-96, 1974
- Wu, P., & Peltier, W. R., "Glacial isostatic adjustment and the free air gravity anomaly as a constraint on deep mantle viscosity", *Geophysical Journal International*, 74(2), 377-449, 1983.